

Anisotropy of unsaturated hydraulic properties of compacted mineral capping systems seven years after construction

Steffen Beck-Broichsitter^{a,*}, Heiner Fleige^b, Jaromir Dusek^c, Horst H. Gerke^a

^a Working Group "Hydropedology", Research Area 1 "Landscape Functioning", Leibniz Centre for Agricultural Landscape Research (ZALF), Eberswalder Straße 84, 15374 Müncheberg, Germany

^b Institute of Plant Nutrition and Soil Science, Christian-Albrechts-University Kiel, Germany

^c Department of Hydraulics and Hydrology, Faculty of Civil Engineering, Czech Technical University in Prague, Thakurova 7, Prague 166 29, Czech Republic

ARTICLE INFO

Keywords:

Waste capping system
Anisotropy
Matric flow potential
Soil water diffusivity

ABSTRACT

The mechanical compaction of soil material of mineral landfill systems affects the continuity and connectivity of the complex soil pore network. A horizontally-oriented layering is intended to generate a slope-induced lateral water flow out of mineral capping systems that is sufficient to minimise the statutory required vertical percolation through the underlying waste body and the potential leachate.

In this case, soil compaction affects both the porosity and water retention as capacity values and the hydraulic conductivity as intensity parameter. The idea of this study was to combine information on both soil properties in an extended anisotropy factor based on the soil water diffusivity. The analysis is focused on the direction-dependent soil hydraulic properties of a mechanically compacted landfill capping system.

In particular, the volume fractions were related to the fractional capillary potential for each of the characteristic pore size classes. Three different soil profiles of top, middle, and bottom slopes of the mineral capping system of the Rastorf landfill in Northern Germany were sampled seven years after construction. Undisturbed soil cores of 100 cm³ and 438 cm³ were extracted in vertical (ver) and horizontal directions (hor) in depths of 20, 50, and 80 cm representing the main layers. The soil water retention and unsaturated hydraulic conductivity, K, functions were determined by suction plates, permeameter, and the evaporation method. In the coarse pores range (pressure head values of $h \geq -300$ hPa), the standard anisotropy ratio, AR, $(K(\text{Se})_{\text{hor}}/K(\text{Se})_{\text{ver}})$ as a function of effective saturation, Se, in the sealing liner in 80 cm depth was larger than 1, indicating higher horizontal than vertical K(Se) values. Thus, AR-values above 1 in the range close to water saturation especially in 80 cm depth suggest the tendency of lateral water flow out of mineral capping system due to a sufficient hydraulic potential and thus its reasonable functionality, even seven years after construction.

The anisotropy factor was extended in two steps; for AR* and AR**, the pore size class-related matric flux potential, ϕ , and the soil water diffusivity, $D(\theta)$, were proposed to combine intensity parameters with capacity-based volume fractions of pore size classes and the fractional capillary potential. The ϕ - and $D(\theta)$ -weighted anisotropy ratios, AR* and AR**, indicate that anisotropy increases with the volume fraction of macropores ($r_{\text{AR}^*}^2$ of 0.69–0.77; $r_{\text{AR}^{**}}^2$ of 0.71–0.80) and wide coarse pores ($r_{\text{AR}^*}^2$ of 0.57–0.78; $r_{\text{AR}^{**}}^2$ of 0.79–0.89) in both directions. The results suggest that by combining both the intensity and the capacity parameters of the soil hydraulic properties in an extended anisotropy ratio improves the information on compacted mineral capping systems.

1. Introduction

Landfills still represent the major option of global waste disposal, and in Germany the qualitative criteria and technical standards for landfill capping systems are legally fixed and defined by the [German Landfill Directive \(2009\)](#). The major aim of mineral capping systems is

to restrain gas migration and to minimise the leachate generation (precipitation water contaminated with heavy metals or hydrocarbons) into the waste body ([Beck-Broichsitter et al., 2020a](#)).

The idea of mineral capping systems is to substitute synthetic polymers to enable the sustainable use of natural resources. An effective way to minimise the leachate generation represents the layered and

* Corresponding author.

E-mail address: steffen.beck-broichsitter@zalf.de (S. Beck-Broichsitter).

<https://doi.org/10.1016/j.still.2020.104702>

Received 3 April 2020; Received in revised form 18 May 2020; Accepted 26 May 2020

Available online 31 July 2020

0167-1987/ © 2020 The Author(s). Published by Elsevier B.V. This is an open access article under the CC BY license (<http://creativecommons.org/licenses/by/4.0/>).

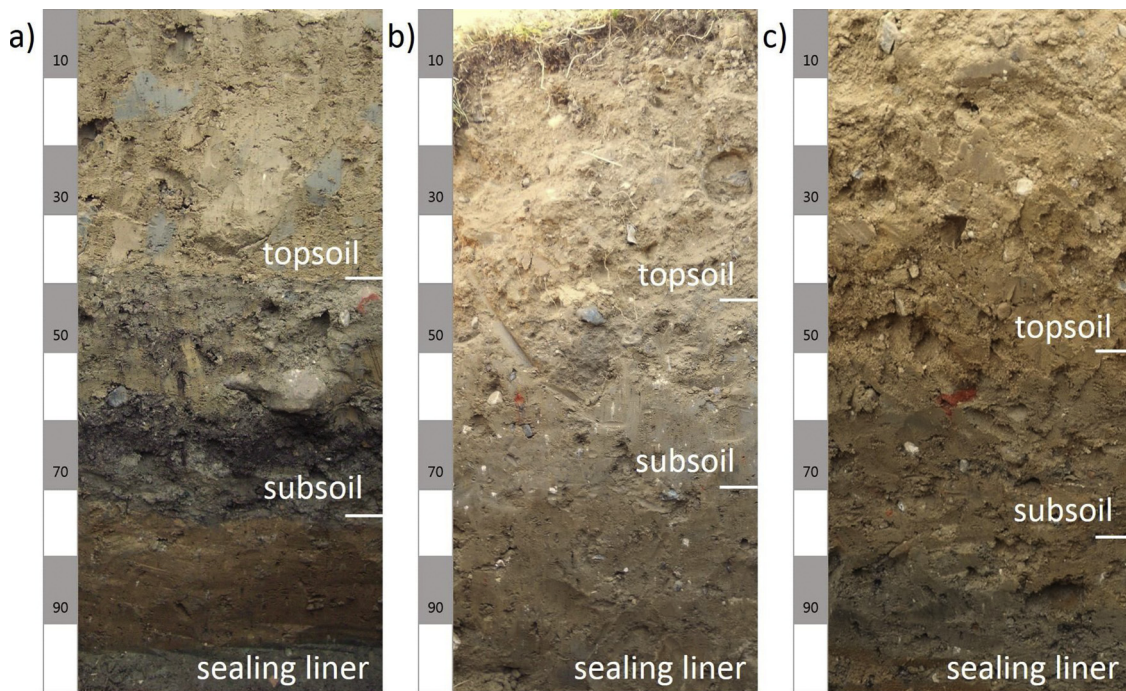


Fig. 1. Photos of soil profiles at Rastorf landfill of a) top (hilltop), b) middle (hillside), and c) bottom (toeslope) slopes of a mineral capping system indicating the topsoil layer (approx. 0–40 cm soil depth), the subsoil layer (approx. 40–70 cm), and the sealing liner in approximately 70–100 cm soil depth. Photos were taken by S. Beck-Broichsitter in 2015.

compacted capping system of low-shrinkage soil material (Beck-Broichsitter et al., 2018b). Soil compaction may affect the soil function, when the induced mechanical stresses exceed the mechanical strength of the soil structure (Zink et al., 2011), resulting in changes of capacity parameters like the total pore volume (especially macropores) and intensity parameters with lower saturated, but relatively higher unsaturated hydraulic conductivity (Horn et al., 2014).

In fact, soil compaction affects both the porosity and water retention as capacity values and the hydraulic conductivity as intensity parameter (Horn and Kutilek, 2009). Information on both soil properties is already combined in the soil water diffusivity; however, the standard anisotropy factors have been based on the soil hydraulic conductivity (Dörner and Horn, 2006). Recently, the anisotropy coefficient has been described as log-linearly proportional to the effective saturation (Zhang, 2014), which simplified the estimation of the saturation-dependent anisotropy relations.

Previous studies focused on the properties of three compacted layers with predominant prismatic-platy structure in soil profiles at the top, middle and bottom slopes of the mineral capping system in Rastorf (Northern Germany) Beck-Broichsitter et al., 2018b, 2020a); the mineral capping system was designed such that lateral water flow decreased the percolation rate towards the underlying waste body and minimized the leachate generation. The degree of compaction as a result of machinery traffic during installation in terms of the pre-compression stress gradually increased from the topsoil layer with 112 kPa downwards to values of 122 kPa in the subsoil layer and up to 136 kPa in the sealing liner (Beck-Broichsitter et al., 2018b). Such compacted layers can also be observed in case of agriculturally used soils (i.e., plough pans) exposed to long-term tillage practices (e.g., Schlüter et al., 2018).

Soil compaction is also affecting the direction-dependent behaviour of intensity parameters (Reszkowska et al., 2011) and in case of mineral capping systems, the compaction-dependent platy structure of the mineral layer material tends to a more anisotropic behaviour of air- and water permeability (e.g., Beck-Broichsitter et al., 2020a, b) as also known for plough pans (Dörner and Horn, 2006). The permeability is

anisotropic if it is different for different directions (Zhang, 2014). Thus, more pronounced horizontal than vertical pathways can effectively result in a lateral water flow out of mineral capping systems in the long run (Beck-Broichsitter et al., 2018a). However, deep-rooting plants (Fan et al., 2016), worm burrows (Soracco et al., 2015), and shrinkage cracks in clay rich materials (Dörner and Horn, 2009) can enhance the formation of vertical cracks and flow pathways resulting in the decrease of lateral flow and functionality of the mineral layer.

The idea of this study was to combine information on both the capacity values and intensity soil parameters in an extended anisotropy factor that is based on the soil water diffusivity. The aim was to identify if initial compaction of the layer material retained a predominant and continuous horizontal-oriented soil pore structure seven years after construction. Thus, the anisotropy in the hydraulic conductivity, $K(h)$, and the soil water diffusivity, $D(\theta)$, that combines intensity ($K(\theta)$) and capacity (water retention function, $h(\theta)$) soil parameters, should vary depending on the pore sizes. Higher $K(h)$ -values in the macropore-size range are expected for the horizontal direction, while vertical $K(h)$ -values should be higher in the medium and fine pore size range.

The focus is on the effect of compaction on the soil structure and the direction-dependency of the unsaturated hydraulic properties. The authors hypothesize that the compacted soil of the mineral capping system is characterised by an anisotropic behaviour of (i) the unsaturated hydraulic conductivity and (ii) soil water diffusivity, or (iii) the combination of both. The results could also help analysing if the mineral capping system fulfils its intended function seven years after construction.

The analysis focused on data from mechanically compacted soil profiles at three hillslope positions as the test case.

2. Materials and methods

2.1. Site and soil

The Rastorf landfill in Schleswig-Holstein (Northern Germany) was actively operated from February 1977 to May 2005; during this period,

Table 1

Basic soil characteristics of the profiles of the top, middle, and bottom slopes in depths of 20, 50, and 80 cm; organic carbon content (OC), pH (CaCl₂) values, soil texture, sand (2–0.063 mm), silt (0.063–0.002 mm), and clay (< 0.002 mm) contents, and solid particle density (ρ_s) in vertical (ver) and horizontal (hor) sampling direction; mean values and standard deviations (\pm symbol) from 3 replicates.

| | depth cm | pH _{CaCl2} – | OC g kg ⁻¹ | Sand g kg ⁻¹ | Silt g kg ⁻¹ | Clay g kg ⁻¹ | ρ_s g cm ⁻³ |
|--------------|-------------|--------------------------|--------------------------|----------------------------|----------------------------|----------------------------|--------------------------------|
| top slope | 20 | 7.36 \pm 0.1 | 1.25 \pm 0.3 | 690 \pm 20 | 190 \pm 5 | 120 \pm 5 | 2.64 \pm 0.1 |
| | 50 | 7.66 \pm 0.2 | 1.25 \pm 0.3 | 680 \pm 10 | 200 \pm 10 | 120 \pm 5 | 2.62 \pm 0.4 |
| | 80 | 7.58 \pm 0.1 | 1.75 \pm 0.1 | 660 \pm 10 | 210 \pm 5 | 130 \pm 5 | 2.63 \pm 0.1 |
| middle slope | 20 | 7.57 \pm 0.2 | 1.27 \pm 0.2 | 650 \pm 10 | 210 \pm 5 | 140 \pm 10 | 2.64 \pm 0.1 |
| | 50 | 7.67 \pm 0.1 | 1.32 \pm 0.2 | 660 \pm 20 | 210 \pm 15 | 130 \pm 5 | 2.62 \pm 0.2 |
| | 80 | 7.52 \pm 0.05 | 2.12 \pm 0.2 | 720 \pm 15 | 180 \pm 10 | 100 \pm 5 | 2.61 \pm 0.1 |
| bottom slope | 20 | 7.60 \pm 0.1 | 1.54 \pm 0.4 | 640 \pm 10 | 220 \pm 10 | 140 \pm 5 | 2.64 \pm 0.1 |
| | 50 | 7.70 \pm 0.05 | 1.61 \pm 0.2 | 650 \pm 10 | 220 \pm 10 | 140 \pm 10 | 2.63 \pm 0.1 |
| | 80 | 7.44 \pm 0.2 | 1.50 \pm 0.1 | 640 \pm 20 | 220 \pm 5 | 140 \pm 10 | 2.63 \pm 0.2 |

Table 2

Volume fractions of pore sizes for macropores (MaP) with $d > 0.3$ mm, wide coarse pores (wCP) with $0.3 < d > 0.05$ mm, narrow coarse pores (nCP) with $0.05 < d > 0.01$ mm, medium pores (MP) with $0.01 < d > 0.0002$ mm, and fine pores (FP) with $d \leq 0.0002$ mm, and the dry bulk density, ρ_b (g cm⁻³), of the soil profiles of top, middle, and bottom slopes in depths of 20, 50, and 80 cm and sampling direction (ver = vertical, hor = horizontal); mean and standard deviations (\pm symbol) from 5 replicates.

| | depth cm | | MaP cm ³ cm ⁻³ | wCP cm ³ cm ⁻³ | nCP cm ³ cm ⁻³ | MP cm ³ cm ⁻³ | FP cm ³ cm ⁻³ | ρ_b g cm ⁻³ |
|--------------|-------------|-----|---|---|---|--|--|--------------------------------|
| top slope | 20 | ver | 0.021 \pm 0.005 | 0.027 \pm 0.007 | 0.048 \pm 0.003 | 0.078 \pm 0.01 | 0.122 \pm 0.01 | 1.90 \pm 0.06 |
| | | hor | 0.022 \pm 0.003 | 0.051 \pm 0.006 | 0.049 \pm 0.006 | 0.077 \pm 0.008 | 0.094 \pm 0.01 | 1.85 \pm 0.11 |
| | 50 | ver | 0.020 \pm 0.003 | 0.029 \pm 0.005 | 0.038 \pm 0.004 | 0.077 \pm 0.01 | 0.136 \pm 0.02 | 1.80 \pm 0.08 |
| | | hor | 0.024 \pm 0.004 | 0.037 \pm 0.006 | 0.043 \pm 0.005 | 0.074 \pm 0.013 | 0.100 \pm 0.01 | 1.90 \pm 0.04 |
| | 80 | ver | 0.023 \pm 0.002 | 0.022 \pm 0.007 | 0.027 \pm 0.002 | 0.069 \pm 0.011 | 0.204 \pm 0.012 | 2.04 \pm 0.08 |
| | | hor | 0.028 \pm 0.002 | 0.031 \pm 0.003 | 0.029 \pm 0.003 | 0.070 \pm 0.009 | 0.139 \pm 0.018 | 2.01 \pm 0.03 |
| middle slope | 20 | ver | 0.0236 \pm 0.004 | 0.016 \pm 0.003 | 0.022 \pm 0.006 | 0.087 \pm 0.005 | 0.136 \pm 0.008 | 1.91 \pm 0.06 |
| | | hor | 0.0238 \pm 0.003 | 0.012 \pm 0.001 | 0.026 \pm 0.003 | 0.085 \pm 0.01 | 0.112 \pm 0.01 | 1.93 \pm 0.07 |
| | 50 | ver | 0.0248 \pm 0.005 | 0.039 \pm 0.003 | 0.025 \pm 0.004 | 0.062 \pm 0.012 | 0.143 \pm 0.006 | 1.88 \pm 0.08 |
| | | hor | 0.0228 \pm 0.005 | 0.047 \pm 0.002 | 0.030 \pm 0.005 | 0.055 \pm 0.01 | 0.116 \pm 0.01 | 1.93 \pm 0.07 |
| | 80 | ver | 0.0195 \pm 0.006 | 0.015 \pm 0.002 | 0.019 \pm 0.003 | 0.053 \pm 0.01 | 0.158 \pm 0.014 | 1.82 \pm 0.1 |
| | | hor | 0.0225 \pm 0.004 | 0.023 \pm 0.005 | 0.020 \pm 0.002 | 0.052 \pm 0.01 | 0.140 \pm 0.01 | 2.00 \pm 0.09 |
| bottom slope | 20 | ver | 0.0268 \pm 0.006 | 0.019 \pm 0.005 | 0.035 \pm 0.003 | 0.086 \pm 0.018 | 0.158 \pm 0.012 | 1.93 \pm 0.06 |
| | | hor | 0.0212 \pm 0.006 | 0.022 \pm 0.003 | 0.043 \pm 0.003 | 0.087 \pm 0.02 | 0.142 \pm 0.02 | 1.96 \pm 0.06 |
| | 50 | ver | 0.0271 \pm 0.005 | 0.019 \pm 0.006 | 0.013 \pm 0.002 | 0.078 \pm 0.016 | 0.155 \pm 0.018 | 1.79 \pm 0.06 |
| | | hor | 0.0255 \pm 0.005 | 0.019 \pm 0.002 | 0.013 \pm 0.002 | 0.078 \pm 0.015 | 0.147 \pm 0.01 | 1.82 \pm 0.08 |
| | 80 | ver | 0.0212 \pm 0.004 | 0.018 \pm 0.003 | 0.023 \pm 0.003 | 0.079 \pm 0.01 | 0.142 \pm 0.02 | 1.90 \pm 0.05 |
| | | hor | 0.0222 \pm 0.004 | 0.020 \pm 0.002 | 0.022 \pm 0.004 | 0.089 \pm 0.02 | 0.124 \pm 0.016 | 1.85 \pm 0.06 |

Table 3

Values of the Akaike Information Criterion (AICc) obtained from fitting the unimodal (van Genuchten, 1980) and bimodal (Durner, 1994) soil water retention models to data from top, middle, and bottom slopes in depths of 20, 50, and 80 cm and sampling direction (ver = vertical, hor = horizontal).

| SWRC | depth cm | top slope | | middle slope | | bottom slope | |
|----------|-------------|-----------|------|--------------|-----|--------------|-----|
| | | ver | hor | ver | hor | ver | hor |
| unimodal | 20 | -98 | -93 | -85 | -83 | -89 | -87 |
| | 50 | -99 | -95 | -99 | -93 | -95 | -80 |
| | 80 | -98 | -106 | -98 | -90 | -100 | -90 |
| bimodal | 20 | -58 | -55 | -63 | -59 | -57 | -36 |
| | 50 | -57 | -44 | -54 | -49 | -65 | -76 |
| | 80 | -65 | -64 | -59 | -58 | -59 | -58 |

about 2.0 million tons of municipal domestic wastes were deposited. The landfill can be divided into a top slope (hilltop) (latitude 54°28'N, longitude 10°32'E), middle slope (hillside) (54°28'N, 10°32'E) and bottom slope (toeslope) (54°28'N, 10°32'E) with a steepness of the slopes between 14 and 16°, respectively. In 2008, a mineral capping system consisting of three differently-compacted glacial till-derived layer/liner was installed by an excavator and mechanically compacted by using a smoothing roller (Beck-Broichsitter et al., 2018b). Thus, the soil profiles for each slope can be divided into the topsoil layer (approx. 0–40 cm soil depth), subsoil layer (approx. 40–70 cm), and the low-

permeable sealing liner in approx. 70–100 cm soil depth, respectively (Fig. 1). The soil profiles can be characterised as Stagnosols (A/Bg/2Bg horizons) according to FAO soil classification (IUSS Working Group WRB, 2014). A circumferential drainage system collects the interflow and therefore the lateral-induced leachate flow. An additional drainage system above the bottom sealing system in 20 m depth collects the leachate and therefore the contaminants, which thereafter is treated (osmosis) before being discharged into the natural water body (Widomski et al., 2015; Beck-Broichsitter et al., 2018a).

The study site is characterised by a maritime climate with an annual average precipitation rate of 720 mm year⁻¹ and an annual mean temperature of 8.9 °C between 2008 and 2015. The site is used as pasture with a dominant share of cocksfoot (*Dactylis glomerata* L.); red fescue (*Festuca rubra* L.); meadow grass (*Poa pratensis* L.), the biomass growth is managed by mowing 2-times a year (Beck-Broichsitter et al., 2018a).

In 2015, 180 undisturbed soil cores (diameter: 5.5 cm, height: 4 cm, approx. 100 cm³) and 72 larger cores (diameter: 10 cm, height: 6 cm, approx. 480 cm³) were collected from three profiles of the mineral capping system in three depths of 20, 50, and 80 cm. Sampling was carried out in vertical (0°; n = 10 per soil depth) and horizontal (90°; n = 10 per soil depth) directions, respectively.

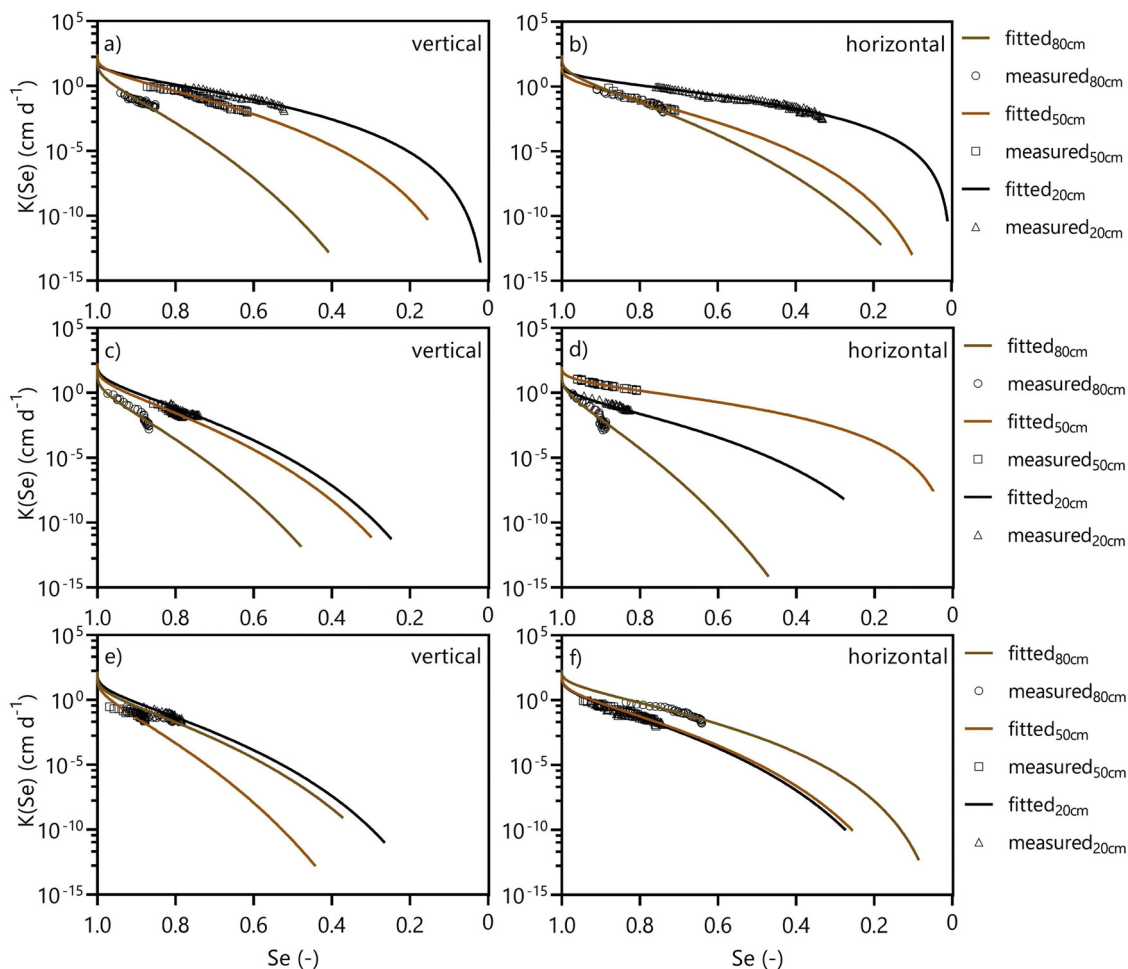


Fig. 2. Single fits from the mean of four data points obtained with HYPROP software of the unimodal unsaturated hydraulic conductivity $K(Se)$ (Priesack and Durner, 2006) of top (a,b), middle (c,d), and bottom (e,f) slopes in depths of 20, 50, and 80 cm and sampling direction (ver = vertical, hor = horizontal).

2.2. Soil physical and hydraulic properties

The undisturbed soil cores and disturbed material were collected from three soil profiles (Fig. 1) of the mineral capping system located at the top, middle, and bottom slopes of the mineral capping system. The disturbed soil material was from the direct surrounding of the intact cores that were sampled for determination of soil hydraulic properties. The sand, silt, and clay content was analysed by wet sieving ($> 63 \mu\text{m}$) and pipette method ($\leq 63 \mu\text{m}$); solid particle density, ρ_s (g cm^{-3}), was determined with pycnometers, organic carbon was analysed with coulometric carbon dioxide (CO_2) measurements on disturbed soil material in 3 replicates per depth (Hartge and Horn, 2016). The saturated hydraulic conductivity, K_s (cm d^{-1}), was determined with falling-head method, values of dry bulk density, ρ_b (g cm^{-3}), and volumetric soil water content, θ ($\text{cm}^3 \text{cm}^{-3}$), were obtained from intact soil cores of 100 cm^3 with 5 replicates per soil depth and sampling direction. Nearly saturated samples were dehydrated with suction plate for applied pressure heads, h , of -30 , -60 , -150 , -300 , and -500 hPa, with a pressure chamber at $-15,000$ hPa, and by drying at 105°C for 24 h (Blake and Hartge, 1986) to determine ρ_b values.

The unsaturated soil hydraulic conductivity, $K(h)$, was determined with the evaporation method in 4 replicates for each soil depth and direction as follows. The intact soil cores (480 cm^3) were carefully wetted from the bottom and placed on a sample holder. Two time-domain-reflectometry sensors and two automatically recording pressure transducer tensiometers were installed horizontally in 1.0 cm and 5.0 cm distance from the bottom. The temporal changes in water

contents and pressure heads were automatically recorded every 15 min in the range of about $-600 \text{ hPa} < h < -10 \text{ hPa}$. The samples regularly dried out to about -500 hPa (lower tensiometer) and -600 hPa (upper tensiometer). The h -values at the upper, $h_u(t)$, and the lower, $h_l(t)$, tensiometers were used to determine the hydraulic gradient, i_m (cm cm^{-1}), per time interval, $\Delta t = t_0 - t_{\text{end}}$ (min), along the vertical distance, Δz , between both tensiometers as proposed by Schindler (1980) and Wendroth et al. (1993).

$$i_m = \frac{1}{2} \left(\frac{h_u(t_0) - h_l(t_0)}{\Delta z} + \frac{h_u(t_{\text{end}}) - h_l(t_{\text{end}})}{\Delta z} \right) - 1 \quad (1)$$

The values of the hydraulic conductivity, $K(h^*)$, were obtained by assuming a linear water content profile within the sample considering a zero flux at the bottom of the soil core (Schindler, 1980; Wendroth et al., 1993).

$$K(h^*) = \frac{\Delta V}{2A_{\text{sc}} \cdot \Delta t \cdot i_m} \quad (2)$$

where A_{sc} (cm^2) is the cross-sectional area of the soil core (80 cm^2), ΔV (cm^3) is the TDR-derived loss in water volume, and h^* is the mean value of the pressure heads of the two tensiometers (i.e., $h^* = 0.5(h_u + h_l)$) with $\Delta t = 15$ min. Without any fixed value in the wet range, the gradient, i_m , varied at minimum between 0.4 and 0.8 cm cm^{-1} .

The HYPROP software (Pertassek et al., 2011) was used for fitting the observed data to obtain continuous functions $K(h)$ and $h(\theta)$ for the vertical and horizontal samples of top, middle, and bottom slopes in depths of 20, 50, and 80 cm.

The observed water retention data were fitted with the constraint

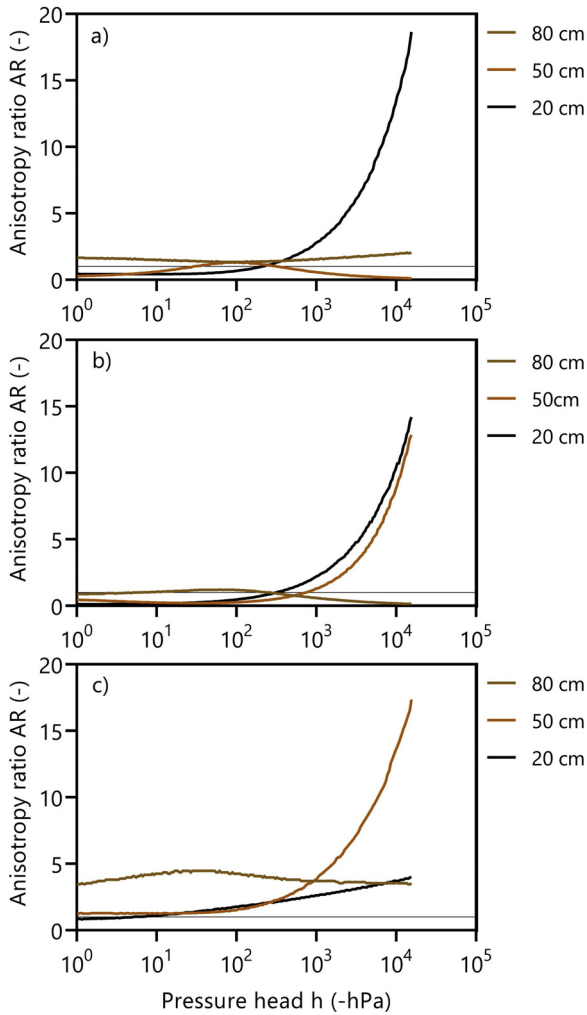


Fig. 3. Anisotropy ratio AR ($K(\text{Se})_{\text{hor}}/K(\text{Se})_{\text{ver}}$) as a function of the pressure head (-hPa) of top (a), middle (b), and bottom (c) slopes in depths of 20, 50, and 80 cm.

unimodal (van Genuchten, 1980) and bimodal van Genuchten models (Durner, 1994):

$$\text{Se}(h) = \frac{\theta - \theta_r}{\theta_s - \theta_r} = \begin{cases} \sum_{i=1}^2 w_i \left[1 + (\alpha_i h)^{n_i} \right]^{-m_i} & \text{for } h < 0 \\ 1 & \text{for } h \geq 0 \end{cases} \quad (3)$$

where $\text{Se}(h)$ is the effective saturation (-), θ_s is saturated and θ_r is residual water content ($\text{cm}^3 \text{cm}^{-3}$), α (cm^{-1}), n (-) and m (-), with $m = 1 - 1/n$, are empirical parameters for both pore domains (index i), and w_i is a pore-domain weighting factor (bimodal: $w_1 = 1 - w_2$, unimodal: $w_2 = 0$).

The unsaturated hydraulic conductivity $K(\text{Se})$ was determined with the Mualem-van Genuchten (MvG) type analytical function and the bimodal retention function (Priesack and Durner, 2006):

$$K(\text{Se}) = K_s \left(\sum_{i=1}^k w_i \text{Se}_i \right)^\tau \left(\frac{\sum_{i=1}^k w_i \alpha_i \left[1 - (1 - \text{Se}_i^{1/m_i})^{m_i} \right]}{\sum_{i=1}^k w_i \alpha_i} \right)^2 \quad (4)$$

where integer k denotes the modality of the model (i.e., $k = 2$ for bimodal), w_i is a weighting factor for the sub-curves of each pore domain ($0 < w_i < 1$ and $\sum w_i = 1$), K_s corresponds to the saturated hydraulic conductivity, and τ (-) is the tortuosity.

The soil water retention functions were fitted in a first step and the derived fitting parameters, α , n , m , and K_s were then used in a second step for fitting the $K(\text{Se})$ functions.

The slope of the soil water retention curve, $d\text{Se}/dh$, was used to calculate the pore size distribution (PSD) (Ding et al., 2016). The h -value of -10 hPa (about 9.81 cm water column) was assumed as boundary between a) macropores, b) structural pores (wide coarse pores), and c) textural pores (narrow coarse pores, medium pores, and fine pores) as proposed by Beck-Broichsitter et al. (2020b) considering equivalent pore radii (Eq. 5). The radii, r (cm), of the different pore size classes, i , were determined as follows (Hartge and Horn, 2016):

$$r_i = \frac{0.149}{|h_i|} \quad (5)$$

where h is the pressure head (cm) and the i -th pore size classes consist of macropores ($h_1 \geq -10$ hPa), wide coarse pores ($-10 < h_2 \geq -60$ hPa), narrow coarse pores ($-60 < h_3 \geq -300$ hPa), medium pores ($-300 < h_4 \geq -15,000$ hPa), and fine pores ($h_5 < -15,000$ hPa).

The pore sizes were classified as macropores (MaP) with pore diameters of $d \geq 0.3$ mm, wide coarse pores (wCP) with $0.3 < d \geq 0.05$ mm, narrow coarse pores (nCP) with $0.05 < d \geq 0.01$ mm, medium pores (MP) with $0.01 < d \geq 0.0002$ mm, and fine pores (FP) with $d < 0.0002$ mm.

The anisotropy ratio (AR) is defined as ratio of $K(\text{Se})$ -values obtained in horizontal (hor) and vertical (ver) direction and was calculated as follows:

$$\text{AR} = \frac{K(\text{Se})_{\text{hor}}}{K(\text{Se})_{\text{ver}}} \quad (6)$$

The intensity-capacity concept, proposed by Horn and Kutilek et al. (2009), deals with the question, if and how it is possible to describe and predict intensity values (i.e., hydraulic conductivity, air permeability) with capacity parameter (i.e., bulk density, pore size distribution). Thus, pedotransfer equations based on capacity parameter can only be used to describe and predict various material properties, but not the soil type dependent hydraulic properties including the effect of structure and mechanical strength at different scales (Horn and Kutilek, 2009; Beck-Broichsitter et al., 2020b).

In this study, the pore size class-related matric flux potential, ϕ , and the soil water diffusivity, $D(\theta)$, derived from $K(h)$ function were used for comparing and linking intensity parameter with the capacity-based volume fraction of pore size classes with a pore size-related fraction of the capillary potential.

The matric flux potential, ϕ , ($\text{cm}^2 \text{d}^{-1}$), is the integral of $K(h)$ over h (i. e., Haverkamp and Vauclin, 1981) and is used to represent an effective value of the capillary pull per i -th pore size class. The integration of the $K(h)$ function was carried out numerically for pore size classes, i , as:

$$\phi_i = \int_{h^+}^{h^-} K(h_i) dh \quad (7)$$

where h^+ is the upper and h^- is the lower value of each of the five h -ranges representing MaP, wCP, nCP, MP, and FP. An effective value of the anisotropy ratio, AR_i^* , per pore size class, i , was calculated as:

$$\text{AR}_i^* = \phi_i \int_{h^+}^{h^-} \frac{1}{\text{AR}_i} dh \quad (8)$$

The anisotropy ratios of the pore size class, i , defined in Eq. 8, are weighted by ϕ_i .

The soil water diffusivity, $D(\theta)$ ($\text{cm}^2 \text{d}^{-1}$), is the product of $K(\theta)$ and the differential water capacity, $dh/d\theta$ (i.e., slope of the water retention function), defined as:

$$D(\theta) = K(\theta) \frac{dh}{d\theta} \quad (9)$$

The effective $D(\theta)$ values for the i -th pore size classes were calculated as:

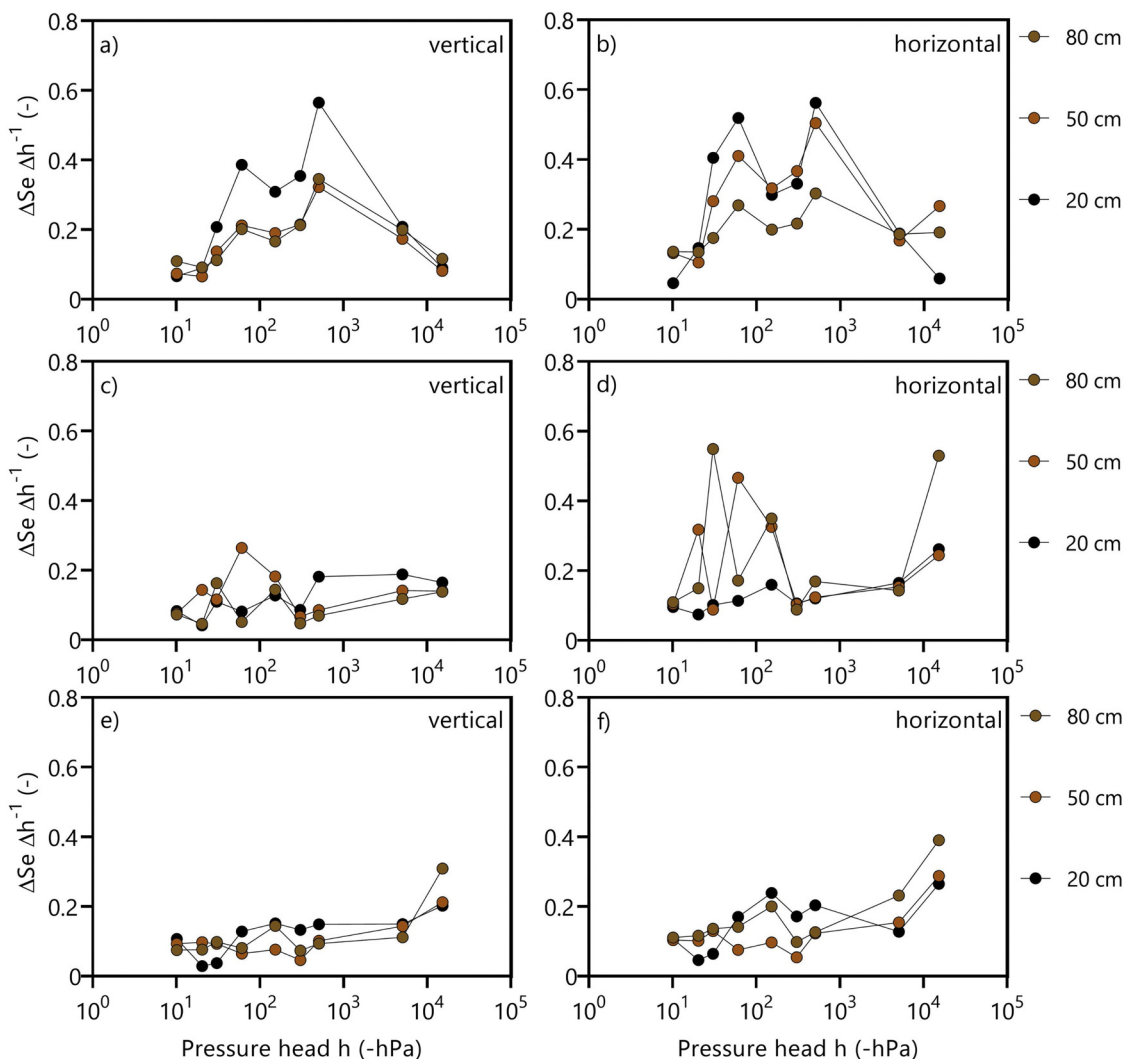


Fig. 4. Relative pore volume fractions at the measured pressure head intervals in terms of the mean slope of the soil water retention curve ($\Delta Se/\Delta h$) per interval for soil profiles of top (a,b), middle (c,d), and bottom (e,f) slopes in depths of 20, 50, and 80 cm and sampling direction (ver = vertical, hor = horizontal).

$$D_i(\theta_i) = \int_{\theta^+}^{\theta^-} K(\theta_i) \frac{dh}{d\theta_i} d\theta \quad (10)$$

where θ^+ (h^+) is the upper and θ^- (h^-) is the lower value of each of the five h -ranges.

A diffusivity-dependent effective value of the anisotropy ratio, AR_i^{**} , per pore size class, i , was calculated as:

$$AR_i^{**} = D_i(\theta_i) \int_{\theta^+}^{\theta^-} \frac{1}{AR_i} d\theta \quad (11)$$

Thus, the effective weighted anisotropy ratio in Eq. 11 combines both, intensity and capacity parameters in form of $D(\theta)$.

2.3. Statistical analyses

The second-order Akaike Information Criterion (Hurvich and Tsai, 1989) for small numbers of samples (AICc) was used to choose the most appropriate MvG model with HYPROP software, defined as:

$$AIC_c = -2(\log\text{-likelihood}) + 2k + \frac{2k(k+1)}{(n-k-1)} \quad (12)$$

where n is the effective sample size and k is the number of estimated parameters. Thus, the smaller the value (i.e., the larger the absolute number), the more appropriate is the model (Peters and Durner, 2008).

The fitting quality in terms of the root mean square error (RMSE) was calculated as:

$$RMSE = \sqrt{\frac{1}{n} \sum_{i=1}^n (K(Se)_{fit} - K(Se)_{obs})^2} \quad (13)$$

where $K(Se)_{fit}$ are fitted and $K(Se)_{obs}$ observed values.

3. Results

3.1. Soil porosity and water retention characteristics

The glacial till is characterised by a clay content between 100 g kg^{-1} and 140 g kg^{-1} , a slightly alkaline character (pH 7.36–7.70) with an organic carbon content (OC) between 1.25 g kg^{-1} and 2.12 g kg^{-1} , and the ρ_s values ranging between 2.61 and 2.64 g cm^{-3} (Table 1).

The ρ_b values range between 1.79 g cm^{-3} and 2.04 g cm^{-3} for both directions, while the volume fraction of macropores, MaP, between $0.014 \text{ cm}^3 \text{ cm}^{-3}$ and $0.032 \text{ cm}^3 \text{ cm}^{-3}$ and wide coarse pores, wCP, between $0.013 \text{ cm}^3 \text{ cm}^{-3}$ and $0.051 \text{ cm}^3 \text{ cm}^{-3}$. The volume fractions of MaP and wCP tend to be higher in horizontal than in vertical direction (Table 2).

The values of the Akaike Information Criterion (AICc) from fitting uni- and bi-modal vG soil water retention models to data show that the unimodal van Genuchten model is more appropriate (Table 3).

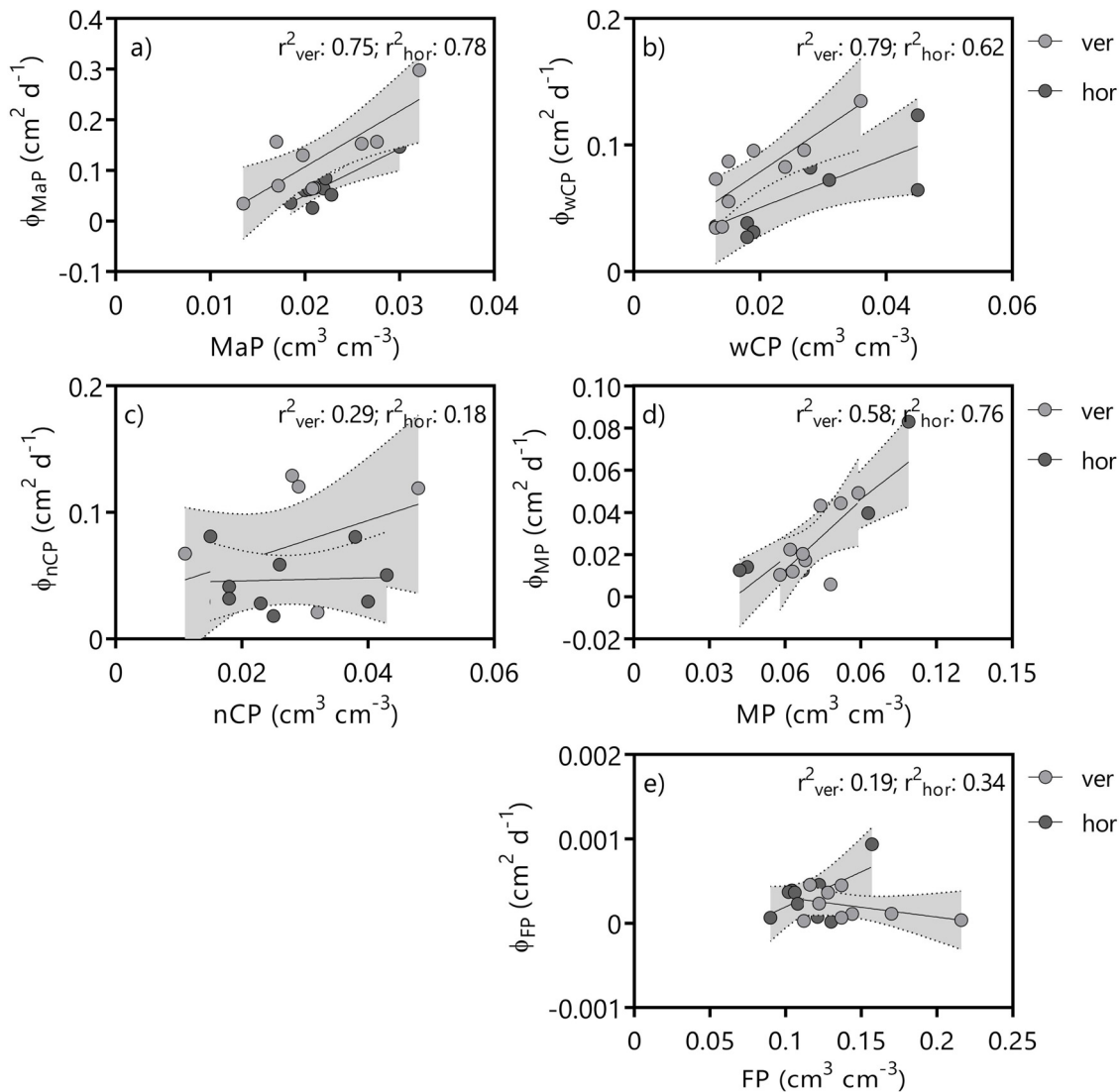


Fig. 5. Matric flux potential, ϕ , versus the volume fraction of pore sizes for macropores (MaP) with $d \geq 0.3$ mm (a), wide coarse pores (wCP) with $0.3 < d \leq 0.05$ mm (b), narrow coarse pores (nCP) with $0.05 < d \leq 0.01$ mm (c), medium pores (MP) with $0.01 < d \leq 0.0002$ mm (d), and fine pores (FP) with $d \leq 0.0002$ mm (e). The dashed line indicates the confidence intervals (CI: 95 %) of the relations between the ϕ -values and the fractional pore sizes (9 data points) in vertical and horizontal directions.

3.2. Unsaturated hydraulic conductivity

From fitting the data obtained with the evaporation method to the unimodal MvG function, the soil from the top, middle and bottom slopes and the different depths shows some direction-dependent differences in the hydraulic conductivity, $K(\text{Se})$, curves (Fig. 2); the $K(\text{Se})$ values are slightly higher in horizontal than in vertical directions in the range of relative saturations (Se) between approx. 0.2 cm d^{-1} and 0.8 cm d^{-1} for all three profiles and depths, respectively. At smaller pressure heads ($h \geq -5$ cm), the $K(\text{Se})$ -values were slightly higher for vertical than for horizontal samples, but differences were not significant.

The goodness-of-fit of the unimodal vG function to the observed $K(\text{Se})$ values was characterised by RMSE values between 0.08 cm d^{-1} and 0.34 cm d^{-1} (Table 5).

The anisotropy ratios (AR) differ between the depths of all three profiles (Fig. 3). In the medium pore range ($-300 < h \leq -15,000$ hPa), the AR values of all profiles in 20 and 50 cm depths are above 1, except for the top slope in 50 cm depth. Thus, the anisotropy in the unsaturated hydraulic conductivity in terms of larger horizontal than vertical $K(\text{Se})$ values was more pronounced in the range of medium

pores. For fine pores ($h < -15,000$ hPa), the AR values were of up to 18.6 (Fig. 3). For the sealing liner in 80 cm depth, the AR values were nearly on the same level between 1.6 and 4.6 for top and bottom slope, while the middle slope indicates AR values below 1 in the medium pores.

The pore size fractions in Fig. 4 show that the samples of the top slope are characterised by a structural peak at -60 hPa and second matric peak at -300 hPa, while the samples of the middle and bottom slopes show two matric peaks at approx. -150 hPa and at around $-15,000$ hPa for all depths and directions, respectively. For all samples, the structural and the first matric peak in horizontal directions is comparatively higher than in vertical direction, while the peaks are more pronounced in 20 cm and 50 cm depth compared to the sealing liner in 80 cm depth (Fig. 4).

The matric flux potential, ϕ , in Fig. 5 indicates a positive slope of the linear relationship for the macropores, wide coarse pores, and medium pores (r^2 of 0.58–0.79), while the narrow coarse pores and fine pores show a weak linear relationship. Thus, the volume fraction of macropores, wide coarse pores, and medium pores predominantly controls the hydraulic conductivity; for the narrow coarse pores (hor) and the fine pores (ver) the opposite seems to be true that more pores

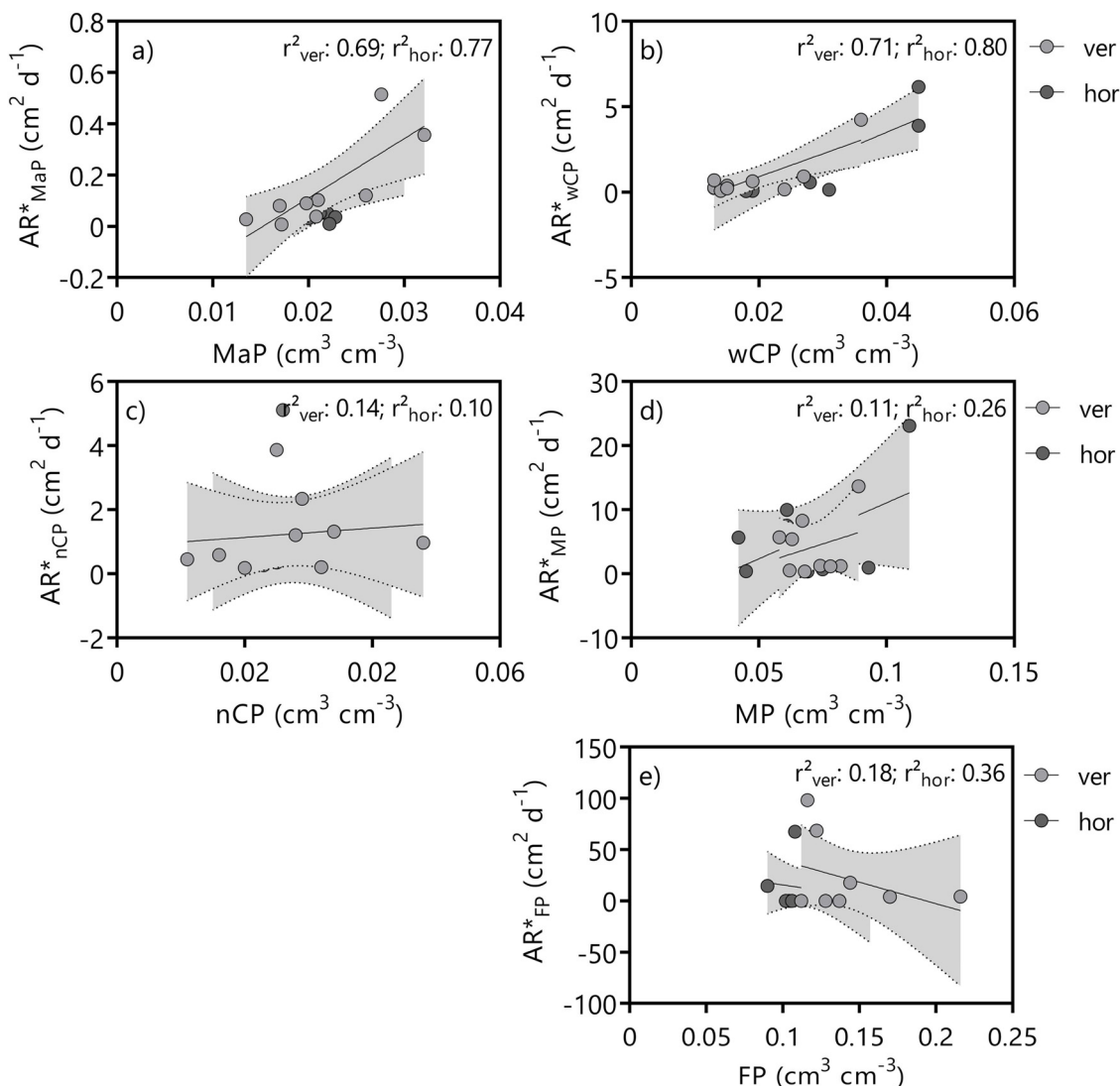


Fig. 6. Mean values of the ϕ -weighted anisotropy ratio, AR^* , versus volume fraction of pore sizes for macropores (MaP) with $d \geq 0.3$ mm (a), wide coarse pores (wCP) with $0.3 < d \leq 0.05$ mm (b), narrow coarse pores (nCP) with $0.05 < d \leq 0.01$ mm (c), medium pores (MP) with $0.01 < d \leq 0.0002$ mm (d), and fine pores (FP) with $d < 0.0002$ mm (e). The dashed lines indicate the confidence intervals (CI: 95 %) of the relations between the ϕ -weighted anisotropy ratio (AR^*) and the pore size fractions fitted to 9 data points in vertical and horizontal direction, respectively.

partially reduce the ϕ -values of that pore size classes (Fig. 5).

For the ϕ -weighted anisotropy ratio, AR^* , defined in Eq. 8, positive relationships were found for the macropores (r^2 of 0.69–0.77) and the wide coarse pores (r^2 of 0.71–0.80) (Fig. 6). Thus, the anisotropy is more pronounced the larger the number of macropores and wide coarse pores is.

3.3. Soil water diffusivity

The soil water diffusivity, $D(\theta)$, as a function of the volume fraction of the pore size classes (Fig. 7) has a positive slope for the linear relationship for the macropores, wide coarse pores, and medium pores (linear regression with an r^2 of 0.59–0.86), while the narrow coarse pores and fine pores show a weak linear relationship with r^2 between 0.11 and 0.21. Thus, the higher the volume fraction of macro pores, wide coarse pores, and medium pores the more pronounced are the $D(\theta)$ values in both directions.

The $D(\theta)$ -weighted anisotropy ratios, AR^{**} , defined in Eq. 11, show positive linear relationships for the macropores (r^2 of 0.57–0.78), wide coarse pores (r^2 of 0.79–0.89), narrow coarse pores (r^2 of 0.09–0.11), and medium pores (r^2 of 0.37–0.52), while the fine pores indicate a

slightly negative linear relationship (r^2 of 0.61–0.23). Thus, the anisotropy increases with the volume fraction of macropores and wide coarse pores in both directions (Fig. 8).

4. Discussion

4.1. Soil physical characteristics: capacity parameter

The peak structure of pore size distribution in Fig. 4 is characterised by a mixture of mono- and bi-peaks (described by unimodal and bimodal pore-size distributions), while a predominant unimodal pore-size distribution is typical for sand-dominated soils (glacial till: 650–720 g kg^{-1}) according to Ding et al. (2016). Thus, the higher the amount of wide coarse pores and medium pores, the more pronounced is the peak structure. Note that the volume fraction of the pore sizes is a scalar and therefore isotropic (e.g., Horn et al., 2014), but the direction-dependent differences in the pore sizes (Table 2) and in the peak structure (Fig. 4) can be related to the small-scale heterogeneity of the soil profiles (Dörner and Horn, 2006; Beck-Broichsitter et al., 2020a). Nevertheless, the chance of capturing a larger volume fraction of the pore sizes is greater for vertically- as compared to horizontally-oriented soil

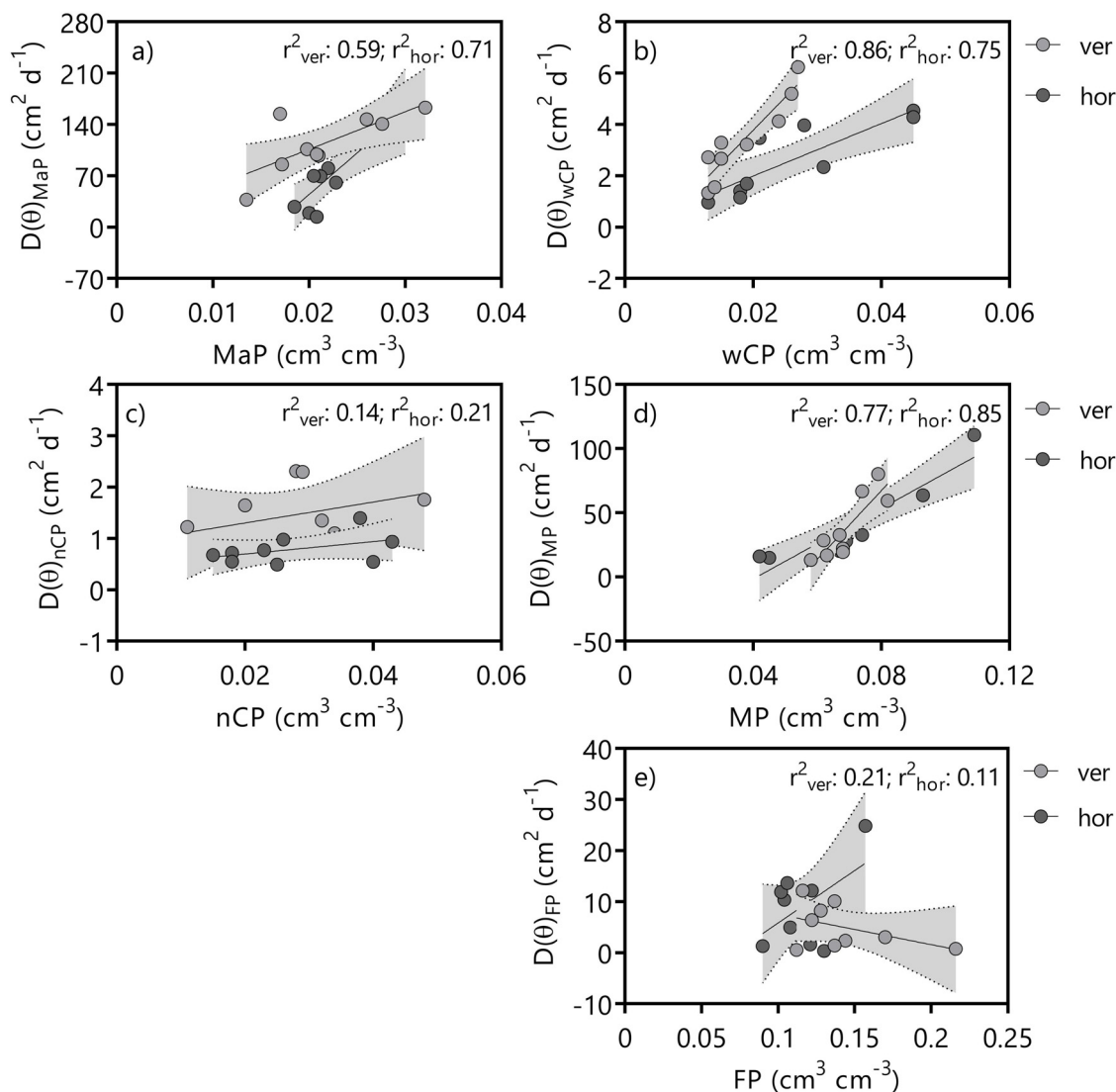


Fig. 7. Mean values of volume fraction of pore sizes versus soil water diffusivity, $D(\theta)$, for macropores (MaP) with $d \geq 0.3$ mm (a), wide coarse pores (wCP) with $0.3 < d \leq 0.05$ mm (b), narrow coarse pores (nCP) with $0.05 < d \leq 0.01$ mm (c), medium pores (MP) with $0.01 < d \leq 0.0002$ mm (d), and fine pores (FP) with $d < 0.0002$ mm (e). The dashed lines indicate the confidence intervals (CI: 95 %) of the relations between the $D(\theta)$ -values and the pore size distribution (pore size) fitted to 9 data points in vertical and horizontal direction, respectively.

sampling.

4.2. Soil physical characteristics: intensity parameter

In addition to the capacity parameters, the functionality of the mineral layer was tested using the functions of soil hydraulic conductivity and soil water diffusivity comparing data of vertically and horizontally extracted soil samples. A platy soil structure was found typical for ploughing-induced compaction of agriculturally used soils in form of a plough pan as interface between topsoil and subsoil in approx. 25–35 cm depth (Schlüter et al., 2018; Beck-Broichsitter et al., 2020b). For the mineral capping system, the predominantly platy structure is a result of the layered and compacted installation (Moon et al., 2008) of the topsoil, subsoil, and the sealing liner (Fig. 1). The soil hydraulic properties can be used as a soil-specific identification of changes in the pore structure (Reszkowska et al., 2011). Moreover, the platy soil structure may result in temporally water-logged soil conditions (Bertolino et al., 2010), while the pronounced slopes between 14 and 16° of the Rastorf landfill (Beck-Broichsitter et al., 2018a) also provide the hydraulic gradient that is needed for lateral subsurface water flow.

The K_s -values (Table 4) range between 27 cm d^{-1} and 276 cm d^{-1} ,

but tend to be higher in vertical as compared to horizontal direction, while the sealing liner in 80 cm depth shows an opposite trend. This anisotropic behaviour can be related to the presence of macropores created by plant roots (Rosolem et al., 2002), worm burrows, and wetting-drying-induced shrinkage cracks resulting in a modified and predominantly vertically-oriented pore network (Horn and Smucker, 2005; Uteau et al., 2013). Therefore, a restrained recovery of the compacted topsoil and subsoil layer in 20 and 50 cm depth can be assumed, while the sealing liner in 80 cm depth seems to be more persistent also after seven years after construction. The persistence is accentuated by leachate rates below 10 % of the annual precipitation (Beck-Broichsitter et al., 2018a), such that 90 % of precipitation is prevented from entering the waste pile.

The direction-dependent differences in $K(\text{Se})$ - and therefore $D(\theta)$ -values were reported to be mostly related to the K_s -values (Germer and Braun, 2015) and pore size distribution (Beck-Broichsitter et al., 2020b). The $K(\text{Se})$ -curves (Fig. 2) indicate a decrease in the hydraulic-conductive flow cross section limiting the water flow in the soil matrix (Reszkowska et al., 2011) and also affecting the pore continuity (Ajayi et al., 2019) with decreasing pressure heads. The smoother decline in the $K(\text{Se})$ values for the soils at 20 cm depth, characterised by

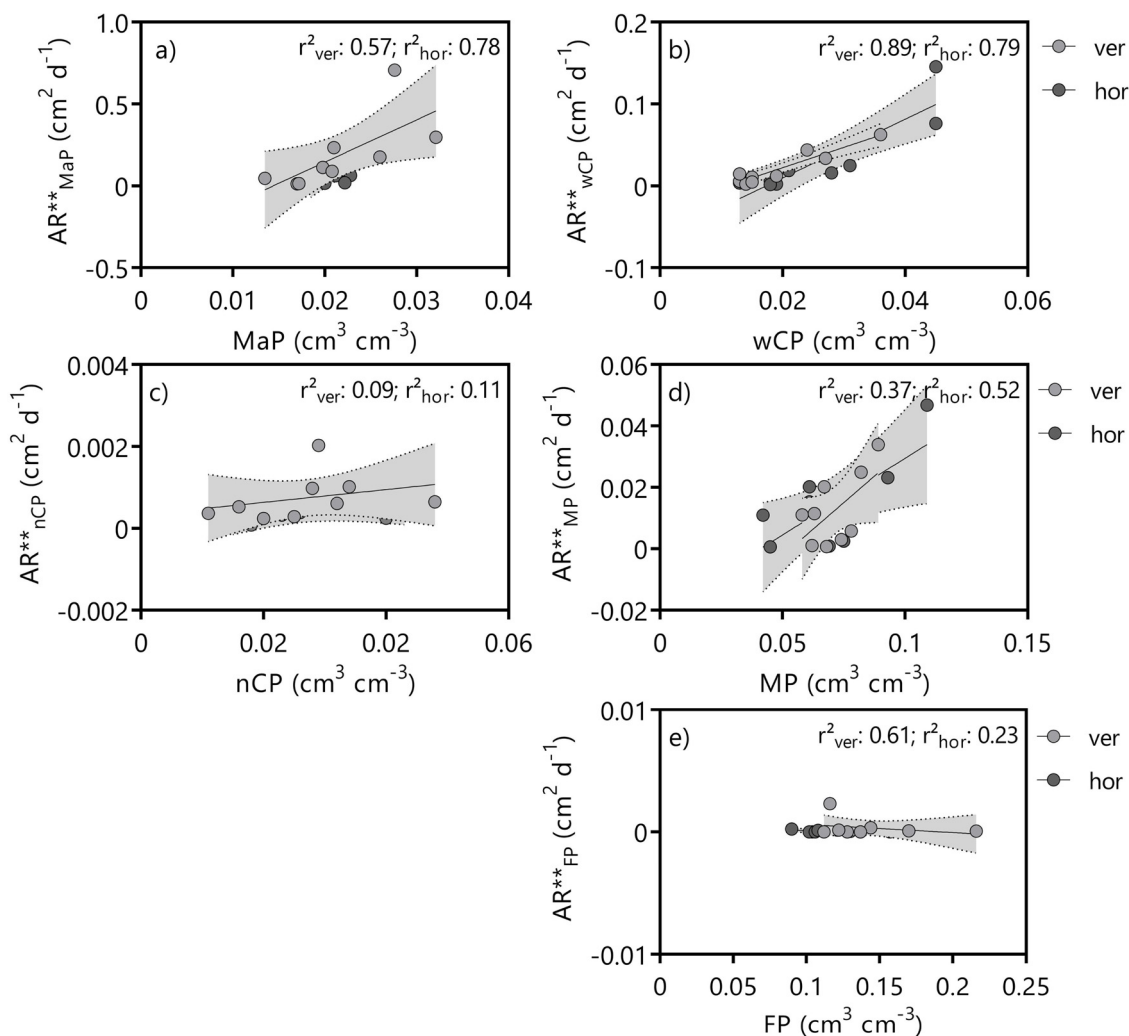


Fig. 8. Mean values of the $D(\theta)$ -weighted anisotropy ratio, AR^{**} , versus the volume fraction of pore sizes for macropores (MaP) with $d \geq 0.3$ mm (a), wide coarse pores (wCP) with $0.3 < d \leq 0.05$ mm (b), narrow coarse pores (nCP) with $0.05 < d \leq 0.01$ mm (c), medium pores (MP) with $0.01 < d \leq 0.0002$ mm (d), and fine pores (FP) with $d < 0.0002$ mm (e). The dashed lines indicate the confidence intervals (CI: 95 %) of the relations between AR^{**} and the volume fraction of pore sizes fitted to 9 data points in vertical and horizontal direction, respectively.

Table 4

Parameters of the van Genuchten soil water retention model and the unimodal unsaturated hydraulic conductivity $K(S_e)$ function obtained by fitting the unimodal ($w_2 = 0$) constrained ($m = 1 - n^{-1}$) with HYPROP software to the mean values of water retention data (four replicates) of top, middle, and bottom slopes in depths of 20, 50, and 80 cm and sampling direction (ver = vertical, hor = horizontal); the τ -values and those of the saturated hydraulic conductivity, K_s , were obtained by fitting the curves to the $K(S_e)$ data in Fig. 2.

| | depth cm | direction | θ_r - $cm^3 cm^{-3}$ - | θ_s | α cm^{-1} | n | K_s $cm d^{-1}$ | τ - |
|--------------|-------------|-----------|----------------------------------|------------|-----------------------|-------|----------------------|-------------|
| top slope | 20 | ver | 0.089 | 0.297 | 0.025 | 1.317 | 96 | 0.11 |
| | | hor | 0.068 | 0.294 | 0.033 | 1.363 | 39 | -2.1 |
| | 50 | ver | 0.029 | 0.299 | 0.051 | 1.143 | 276 | -2.2 |
| | | hor | 0.042 | 0.278 | 0.012 | 1.197 | 49 | 0.98 |
| middle slope | 20 | ver | 0 | 0.344 | 0.027 | 1.072 | 180 | 4.3 |
| | | hor | 0 | 0.299 | 0.035 | 1.096 | 270 | 1.6 |
| | 50 | ver | 0 | 0.272 | 0.023 | 1.113 | 260 | 0.11 |
| | | hor | 0 | 0.261 | 0.012 | 1.110 | 27 | -4.9 |
| bottom slope | 20 | ver | 0.021 | 0.294 | 0.018 | 1.100 | 195 | 0.27 |
| | | hor | 0.085 | 0.271 | 0.113 | 1.217 | 108 | -4.9 |
| | 50 | ver | 0 | 0.265 | 0.018 | 1.061 | 68 | 2.1 |
| | | hor | 0 | 0.252 | 0.011 | 1.065 | 52 | 6.8 |
| 80 | 20 | ver | 0 | 0.335 | 0.064 | 1.100 | 178 | -1.9 |
| | | hor | 0 | 0.335 | 0.044 | 1.210 | 124 | -3.5 |
| | 50 | ver | 0 | 0.289 | 0.015 | 1.069 | 115 | 5.7 |
| | | hor | 0 | 0.279 | 0.020 | 1.112 | 129 | -2.2 |
| 80 | ver | 0 | 0.279 | 0.022 | 1.081 | 155 | -4.6 | |
| | hor | 0 | 0.268 | 0.016 | 1.205 | 219 | 0.62 | |

Table 5

Mean deviation between the fitted and measured data in form of the root mean square error (RMSE) for the unsaturated hydraulic conductivity, $K(\text{Se})$ (cm d^{-1}), of top, middle, and bottom slopes in depths of 20, 50, and 80 cm and sampling direction (ver = vertical, hor = horizontal).

| depth cm | top slope | | middle slope | | bottom slope | |
|-------------|-----------|------|--------------|------|--------------|------|
| | ver | hor | ver | hor | ver | hor |
| 20 | 1.23 | 1.32 | 1.20 | 1.41 | 1.32 | 1.55 |
| 50 | 1.23 | 1.26 | 1.20 | 1.29 | 1.26 | 1.38 |
| 80 | 1.74 | 2.19 | 1.82 | 2.09 | 1.10 | 1.38 |

comparatively higher MvG parameter n (Table 4), indicates a lower water capillary water absorption capacity or a decrease in $K(\text{Se})$ values for the coarse to medium pores (structural to matric peak), that lost their ability to conduct water when drained (Alaoui et al., 2011).

4.3. Anisotropy relations of compacted soils in capping systems

The $K(\text{Se})$ values can be related to the volume fraction of the macropores and the wide coarse pores considering the positive relationship between the matric flow potential and the pore sizes (Fig. 5a,b). This indicates that intensity parameters are functions of pore continuity and connectivity and not directly of capacities such as total pore volume (Dörner and Horn, 2006; Zhang et al., 2006).

With the emptying of the wide coarse pores ($w\text{CP}: \geq -60$ hPa), the AR values in 20 and 50 cm depths strongly increase of up to 18.6, but indicate nearly isotropic or rather slightly higher vertical than horizontal K_s and $K(\text{Se})$ values in the macropore range and therefore a tendency for vertical flow (Zhang, 2014), which is in contrast to the imposed requirements of the layer material. This indicates, that the platy structure at 20 cm and partially in 50 m depths has probably been changed in a prismatic-platy structure as a consequence of annual wetting and drying cycles, macropores created by deep-rooted plant species (Uteau et al., 2013).

In the coarse pores range ($h \geq -300$ hPa), the AR values in the sealing liner in 80 cm depth are above 1 and indicate higher horizontal than vertical $K(\text{Se})$ values. Compared with in-situ pressure head measurements at the Rastorf landfill in 2008–2015 (Beck-Broichsitter et al., 2018b), h -values between -100 hPa and -150 hPa, even during drier periods, enable a sufficient slope-induced lateral water flow out of mineral capping systems (Beck-Broichsitter et al., 2018a), even seven years after installation. The positive relationship between the effective anisotropy ratio, AR^* , and the volume fraction of the macropores and the wide coarse pores in Fig. 6a,b indicates pronounced similarities in the structure of topsoil, subsoil, and sealing liner of the Rastorf landfill.

The soil water diffusivity, $D(\theta)$, used for describing water and energy fluxes in the unsaturated zone (e.g., Espejoa et al., 2014) is combining intensity and capacity parameters. The ratio of $K(\text{Se})$ values to the differential water capacity and therefore the $D(\theta)$ -values can be positively related to the volume fraction of the macropores, wide coarse pores, and medium pores (Fig. 7a,b,d). These relations indicate, that the $D(\theta)$ -values are functions of pore continuity and connectivity and not directly of the pore capacity (Zhang et al., 2006). However, the volume fraction of medium pores (Fig. 7d) indicates a steeper increase in $D(\theta)$ -values for horizontal than for vertical samples and therefore more direction-dependent differences in the soil structure. Nevertheless, the positive relationship between the effective anisotropy ratio, AR^{**} , and the volume fraction of the macropores and wide coarse pores (Fig. 8a,b) indicates similarities in the pore structures created by mechanical compaction of topsoil, subsoil, and sealing liner at all three slope positions.

4.4. Measurement and fitting uncertainties

The AICc values in Table 3 indicate more negative values by using the unimodal vG model (van Genuchten, 1980) compared to the bimodal approach (Durner, 1994). Thus, the more appropriate unimodal MvG model was chosen for the selected data set. The RMSE values are all close to the measurement errors of 1.10 to 2.19 cm d^{-1} for the $K(\text{Se})$ data (Peters and Durner, 2008), and the fitted curves can explain the measurements.

5. Conclusions

The results of this study indicate direction-dependent differences in the soil hydraulic conductivity, the matric flux potential relation, and soil water diffusivity as link between intensity and capacity parameters that strongly depend on the pore size distribution and mostly in the range of macropores to narrow coarse pores. Moreover, the compacted sealing liner with its predominant platy structure tends to a more anisotropic behaviour for the range of macropores to wide coarse pores, resulting in slightly higher saturated and unsaturated hydraulic conductivities in horizontal than in vertical direction. Nevertheless, the soil structure of topsoil and subsoil layers seem to have improved.

The differences between the anisotropy ratio values of layer/liner are relatively small and are therefore mainly characterised by the macro-porosity and the anisotropy - pressure head relations. The anisotropy ratios above 1 in the pressure head range close to water saturation suggest the tendency of supporting subsurface lateral water flow out of the capping system and thus confirm the system's functionality, and this even seven years after installation.

The results the $D(\theta)$ -weighted extended anisotropy ratios, AR^{**} , suggest that by combining both the intensity and the capacity parameters of the soil hydraulic properties in an extended anisotropy ratio improves the information on compacted mineral capping systems. It means for the capping system that AR^{**} values especially in 80 cm depth indicate sufficient potential for lateral flow generation. The study suggests that by weighing the anisotropy ratio with the soil water diffusivity, both the intensity and the capacity parameters of the soil hydraulic properties can be combined.

Acknowledgements

This article is a tribute to Prof. Dr. Rainer Horn's 70th-birthday. We congratulate him and acknowledge his tremendous contributions in the field of soil physics and always encouraging and inspiring discussions.

This study was financially supported by the Innovation Foundation Schleswig-Holstein and the ZMD Rastorf GmbH, Germany.

References

- Ajayi, A.E., Horn, R., Rostek, J., Uteau, D., Peth, S., 2019. Evaluation of temporal changes in hydrostructural properties of regenerating permanent grassland soils based on shrinkage properties and μCT analysis. *Soil Till. Res.* 185 (102), 112. <https://doi.org/10.1016/j.still.2018.09.005>.
- Alaoui, A., Lipiec, J., Gerke, H.H., 2011. A review of the changes in the soil pore system due to soil deformation: a hydrodynamic perspective. *Soil Till. Res.* 115–116, 1–15. <https://doi.org/10.1016/j.still.2011.06.002>.
- Beck-Broichsitter, S., Gerke, H.H., Horn, R., 2018a. Assessment of leachate production from a municipal solid waste landfill through water balance modelling. *Geosciences* 8, 356. <https://doi.org/10.3390/geosciences8100372>.
- Beck-Broichsitter, S., Gerke, H.H., Horn, R., 2018b. Shrinkage characteristics of boulder marl as sustainable mineral liner material for landfill capping systems. *Sustainability* 10, 4025. <https://doi.org/10.3390/su10114025>.
- Beck-Broichsitter, S., Fleige, H., Gerke, H.H., Horn, R., 2020a. Effect of artificial soil compaction in landfill capping systems on anisotropy of air-permeability. *J. Plant Nutr. Soil Sci.* 000, 1–11. <https://doi.org/10.1002/jpln.201900281>.
- Beck-Broichsitter, S., Gerke, H.H., Leue, M., von Jeetze, P.J., Horn, R., 2020b. Anisotropy of unsaturated soil hydraulic properties of eroded Luvisol after conversion to hayfield comparing alfalfa and grass plots. *Soil Till. Res.* 198, 104553. <https://doi.org/10.1016/j.still.2019.104553>.
- Bertolino, A.V.F.A., Fernandes, N.F., Miranda, J.P.L., Souza, A.P., Lopes, M.R.S., Palmieri, F., 2010. Effects of plough pan development on surface hydrology and on soil

- physical properties in Southeastern Brazilian plateau. *J. Hydrol.* 393, 94–104. <https://doi.org/10.1016/j.jhydrol.2010.07.038>.
- Blake, G.R., Hartge, K.H., 1986. Bulk density. In: Klute, A. (Ed.), *Methods of Soil Analysis, Slope 1*, 2nd ed. ASA and SSSA, Madison, WI, USA, pp. 363–375.
- Ding, D., Zhao, Y., Feng, H., Peng, X., Si, B., 2016. Using the double-exponential water retention equation to determine how soil pore-size distribution is linked to soil texture. *Soil Till. Res.* 156, 119–130. <https://doi.org/10.1016/j.still.2015.10.007>.
- Dörner, J., Horn, R., 2006. Anisotropy of pore functions in structured Stagnic Luvisols in the Weichselian moraine region in N Germany. *J. Plant Nutr. Soil Sci.* 169, 213–220. <https://doi.org/10.1002/jpln.200521844>.
- Dörner, J., Horn, R., 2009. Direction-dependent behaviour of hydraulic and mechanical properties in structured soils under conventional and conservation tillage. *Soil Till. Res.* 102, 225–232. <https://doi.org/10.1016/j.still.2008.07.004>.
- Durner, W., 1994. Hydraulic conductivity estimation for soils with heterogeneous pore structure. *Water Resour. Res.* 26, 1483–1496. <https://doi.org/10.1029/93WR02676>.
- Espejoa, A., Giráldezab, J.V., Vanderlindend, K., Taguasc, E.V., Pedrerad, A., 2014. A method for estimating soil water diffusivity from moisture profiles and its application across an experimental catchment. *J. Hydrol.* 514, 161–168. <https://doi.org/10.1016/j.jhydrol.2014.01.072>.
- Fan, J., McConkey, B., Wang, H., Janzen, H., 2016. Root distribution by depth for temperature agricultural crops. *Field Crop. Res.* 189, 68–74. <https://doi.org/10.1016/j.fcr.2016.02.013>.
- German Landfill Directive, 2009. Degree on Landfills (ordinance to Simplify the Landfill Law)—Germany, in the Form of the Resolution of the Federal Cabinet, Dated April 27, 2009. Cabinet of Germany, Berlin, Germany.
- Germer, K., Braun, J., 2015. Determination of anisotropic saturated hydraulic conductivity of a macroporous slope soil. *Soil Sci. Soc. Am. J.* 79, 1528–1536. <https://doi.org/10.2136/sssaj2015.02.0071>.
- Hartge, K.H., Horn, R., 2016. In: Horton, R., Horn, R., Bachmann, J., Peth, S. (Eds.), *Essential Soil Physics, an Introduction to Soil Processes, Structure, and Mechanics*. Schweizerbart Science Publishers, Stuttgart, Germany p. 391.
- Haverkamp, R., Vauclin, M., 1981. A comparative study of three forms of the Richard equation used for predicting onedimension infiltration in unsaturated soil. *Soil Sci. Soc. Am. J.* 45, 13–20.
- Horn, R., Kutilek, M., 2009. The intensity–capacity concept—how far is it possible to predict intensity values with capacity parameters. *Soil Till. Res.* 103, 1–3. <https://doi.org/10.1016/j.still.2008.10.007>.
- Horn, R., Smucker, A., 2005. Structure formation and its consequences for gas and water transport in unsaturated arable and forest soils. *Soil Till. Res.* 82, 5–14. <https://doi.org/10.1016/j.still.2005.01.002>.
- Horn, R., Peng, X., Fleige, H., Dörner, J., 2014. Pore rigidity in structured soils – only a theoretical boundary condition for hydraulic properties? *Soil Sci. Plant Nutr.* 60, 3–14.
- Hurvich, C.M., Tsai, C.L., 1989. Regression and time series model selection in small sample. *Biometrika* 76 (2), 99–104.
- IUSS Working Group WRB, 2014. World reference base for soil resources 2014. International Soil Classification System for Naming Soils and Creating Legends for Soil Maps. World Soil Resources Reports No. 106. FAO, Rome.
- Moon, S., Nam, K., Kim, J.K., Hwan, S.K., Chung, M., 2008. Effectiveness of compacted soil layer as a gas barrier liner in the landfill final cover system. *Waste Manage.* 28, 1909–1914. <https://doi.org/10.1016/j.wasman.2007.08.021>.
- Pertasssek, T., Peters, A., Durner, W., 2011. HYPROP Data Evaluation Software User's Manual, V.1.0, UMS GmbH, Gmunder Str. 37, 81379 München, Germany.
- Peters, A., Durner, W., 2008. A simple model for describing hydraulic conductivity in unsaturated porous media accounting for film and capillary flow. *Water Resour. Res.* 44. <https://doi.org/10.1029/2008WR007136>.
- Priesack, E., Durner, W., 2006. Closed-form expression for the multi-modal unsaturated hydraulic conductivity. *Vadose Zone J.* 5, 121–124. <https://doi.org/10.2136/vzj2005.0066>.
- Reszkowska, A., Krümmelbein, J., Peth, S., Horn, R., Zhao, Y., Gan, L., 2011. Influence of grazing on hydraulic and mechanical properties of semiarid steppe soils under different vegetation type in Inner Mongolia, China. *Plant Soil* 340, 59–72. <https://doi.org/10.1007/s11104-010-0405-3>.
- Rosolem, C., Poloni, J., Tiritan, C., 2002. Root growth and nutrient accumulation in cover crops as affected by soil compaction. *Soil Till. Res.* 65, 109–115. [https://doi.org/10.1016/S0167-1987\(01\)00286-0](https://doi.org/10.1016/S0167-1987(01)00286-0).
- Schindler, U., 1980. Ein Schnellverfahren zur Messung der Wasserleitfähigkeit im teilgesättigten Boden an Stechzylinderproben. *Arch. Acker Pflanzenbau* 24, 1–7.
- Schlüter, S., Großmann, C., Diel, J., Wu, G.-M., Tischer, S., Deubel, A., Rücknagel, J., 2018. Long-term effects of conventional and reduced tillage on soil structure, soil ecological and soil hydraulic properties. *Geoderma* 332, 10–19. <https://doi.org/10.1016/j.geoderma.2018.07.001>.
- Soracco, C.G., Lozano, L.A., Villarreal, R., Palancar, T.C., Collazo, D.J., Sarli, G.O., Filgueira, R.R., 2015. Effects of compaction due to machinery traffic on soil pore configuration. *R. Bras. Ci. Solo.* 39, 408–415. <https://doi.org/10.1590/01000683rbc20140359>.
- Uteau, D., Pagenkemper, S.K., Peth, S., Horn, R., 2013. Root and time dependent soil structure formation and its influence on gas transport in the subsoil. *Soil Till. Res.* 132, 69–76. <https://doi.org/10.1016/j.still.2013.05.001>.
- van Genuchten, M.T., 1980. A closed-form equation for predicting the hydraulic conductivity of unsaturated soils. *Soil Sci. Soc. Am. J.* 44, 892–898.
- Wendroth, O., Ehlers, W., Hopmans, J.W., Kage, H., Halbertsma, J., Wosten, J.H.M., 1993. Reevaluation of the evaporation method for determining hydraulic functions in unsaturated soils. *Soil Sci. Soc. Am. J.* 57, 1436–1443. <https://doi.org/10.2136/sssaj1993.03615995005700060007x>.
- Widomski, M.K., Beck-Broichsitter, S., Zink, A., Fleige, H., Horn, R., 2015. Numerical modeling of water balance for temporary landfill cover in North Germany. *J. Plant Nutr. Soil Sci.* (1999) 178, 401–412. <https://doi.org/10.1002/jpln.201400045>.
- Zhang, Z.F., 2014. Relationship between anisotropy in soil hydraulic conductivity and saturation. *Vadose Zone J.* 13 (6). <https://doi.org/10.2136/vzj2013.09.0172>.
- Zhang, S.L., Grip, H., Lovdahl, L., 2006. Effect of soil compaction on hydraulic properties of two loess soils in China. *Soil Till. Res.* 90 (1-2), 117–125. <https://doi.org/10.1016/j.still.2005.08.012>.
- Zink, A., Fleige, H., Horn, R., 2011. Verification of harmful subsoil compaction in loess soils. *Soil Till. Res.* 114, 127–134. <https://doi.org/10.1016/j.still.2011.04.004>.